

A study of RXTE and BeppoSAX observations of Cyg X-3

A. Szostek* and A. A. Zdziarski*

*Centrum Astronomiczne im. M. Kopernika, Bartycycka 18, 00-716 Warszawa, Poland

Abstract. We present an analysis of Cyg X-3 data from *RXTE*/PCA, HEXTE and ASM, supplemented by a selected spectrum from *BeppoSAX*. We fit the PCA/HEXTE spectra from 1996–2000 by a model including hybrid Comptonization, reflection and absorption, and classify them into hard, intermediate and soft states. Apart from the very strong absorption in Cyg X-3, the spectra resemble those of GRS 1915+105. The soft and intermediate state spectra require the presence of nonthermal Comptonizing electrons. We then study the radiative processes at soft X-rays with a hard-state spectrum from *BeppoSAX* modeled including emission from a photoionized plasma.

INTRODUCTION

Cygnus X-3 is a bright X-ray binary system, located ~ 9 kpc away [13] in the plane of the Galaxy. In spite of its discovery already in 1966 [5], it remains poorly understood. The companion is probably a Wolf-Rayet star with huge mass loss [15]. The nature of the compact object remains unknown.

The system exhibits distinct orbital modulation with a 4.8 hr period, observed both in X-rays and infrared. In radio, Cyg X-3 is the brightest X-ray binary [11], and its very strong radio outbursts indicate the presence of a jet. In X-rays, it exhibits a wide range of variability patterns. On the timescales of months to years, transitions between the hard and soft spectral state occur. The observed lack of ms-timescale variability appears to be due to scattering in the strong wind of the companion [10].

RXTE SPECTRA

We use PCA/HEXTE data from 42 observations in 1996–2000. We use the PCUs 0–2 and the top layer only. We fit each of the PCA/HEXTE spectra with the same model as applied to *INTEGRAL/RXTE* spectra from Cyg X-3 [16]. The model includes Comptonization by hybrid (i.e., both thermal and nonthermal) electrons ([2, 6]), Compton reflection from an ionized medium [9], and absorption by fully and partially covering neutral media. As discussed in [16], this model treats the low-energy part of the spectrum relatively phenomenologically, given the strong absorption taking place in Cyg X-3 and the PCA energy coverage limited to >3 keV. Still, it provides good fits to the PCA/HEXTE spectra and a physical description of the hard X-rays.

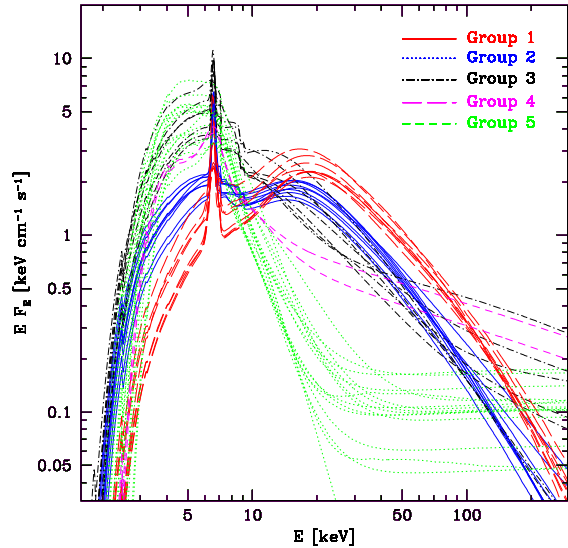


FIGURE 1. Comptonization model spectra of Cyg X-3 from pointed *RXTE* observations. Different line styles correspond to our classification of the spectra, which show a continuity of spectral shapes. Two extreme states, one with a strong soft X-ray emission followed by a weak hard X-ray tail, and one with a weak soft X-ray emission and hard X-rays peaking around ~ 20 keV, are clearly seen.

The obtained model spectra are shown in Fig. 1. We have divided them into five groups ordered by the decreasing flux at 20 keV. The increasing group number also roughly corresponds to the decreasing spectral hardness in the 10–20 keV range. We classify the groups 1–2, 3–4, and 5 as belonging to the hard, intermediate and soft state, respectively. Some of the flux variability within each group is caused by the orbital modulation.

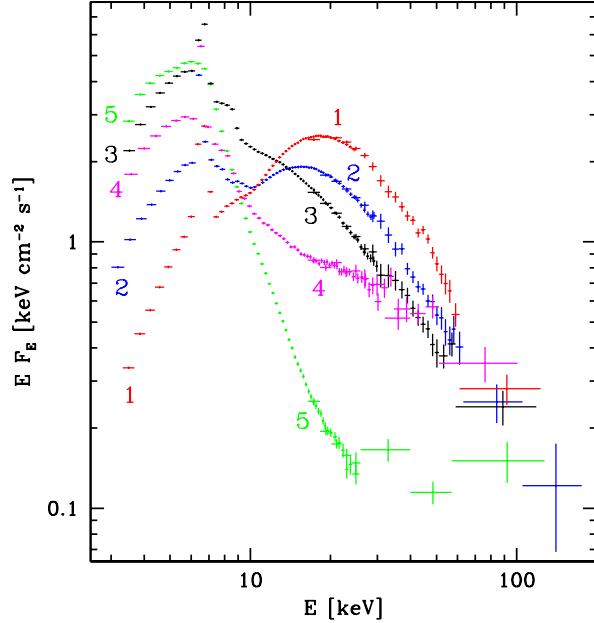


FIGURE 2. Deconvolved spectra for the average of each of the 5 groups shown on Fig. 1, fitted with the same model as the individual spectra. The HEXTE data are renormalized to the level of the PCA.

We have then created average PCA/HEXTE spectra for each group. We have fitted them with the same model as above, obtaining $0.3 < \chi^2_{\nu} < 1.9$ (with a 1% systematic error). The resulting spectra are shown in Fig. 2.

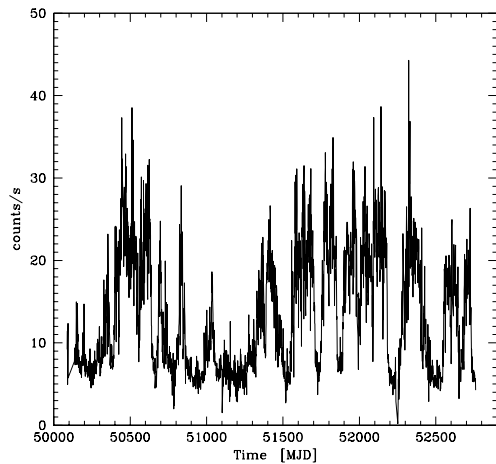


FIGURE 3. The 1.5–12 keV ASM daily-average lightcurve for MJD 50087–52760.

We find that the average spectra require the presence of Comptonizing nonthermal electrons to a varying degree. In the hard state, thermal Comptonization appears to dominate, and the limited high-energy sensitivity of

HEXTE prevents us from obtaining precise constraints on nonthermal electrons. The Cyg X-3 spectra observed in 2002 Dec. by *RXTE* and *INTEGRAL* [16] belong to this state and are closest to our group 2. The intermediate and soft-state spectra are dominated by the disk component Comptonized by a low-temperature plasma, but then followed by a significant hard tail clearly requiring the presence of both hot thermal electrons and nonthermal ones.

Overall, the high-energy parts of the spectra are quite similar to the spectra of GRS 1915+105 shown in [17]. The hard-state spectra are similar to those of the state χ (in the classification of [1]), with the hard X-ray photon indices of $\Gamma \simeq 3$. The soft state spectra are then similar to the spectrum in the γ state of [17], with both objects showing the characteristic hard tail with $\Gamma \simeq 2$. Note that in the case of GRS 1915+105, the presence of nonthermal electrons is required not only in the soft state but also in the hard one. The similarity between the two objects represents a very strong argument for the black-hole nature of the compact object in Cyg X-3.

ASM LIGHTCURVES

On the basis of the *RXTE*/ASM [8] lightcurve (Fig. 3), we can clearly distinguish the hard and soft states similar to those defined above. Here, somewhat arbitrarily, we define the hard and the soft state by the criterion of the countrate smaller and greater than 15 s^{-1} ,

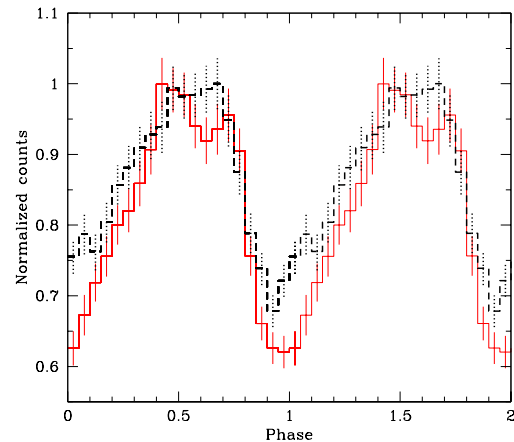


FIGURE 4. The ASM lightcurves folded with the orbital period for the hard and soft state, plotted in the dashed (black) and solid (red) curve, respectively. The period is divided into $20 \times 14.4 \text{ min.}$ bins. Each of the lightcurves is normalized to the respective maximum.

respectively. The resulting (dwell-by-dwell) lightcurves have then been folded with the orbital period using the parabolic ephemeris [14], see Fig. 4.

We find distinct differences in the shape of the two lightcurves. The maximum is broad and flat in the hard state, whereas it forms a sharp peak followed by a secondary one in the soft state. We also see different shapes around the minimum. The differences indicate changes in the source configuration taking place during state transitions. We caution, however, that our criterion to distinguish the states should be phase-dependent as the orbital modulation changes the countrate. Due to this effect, a state with the countrate near 15 s^{-1} gives contribution to either hard or the soft state depending on the phase. We intend to take into account this effect and to study physical implications of the shape of the state-resolved folded lightcurves in the future.

PHASE-RESOLVED RXTE SPECTRA

We consider now three subsequent *RXTE* pointed observations in the hard state in 1996 Aug., see Fig. 5. We have divided the data into 18 parts, each not exceeding in duration 15% of the orbital period. For each part, we have obtained the spectrum, which we then fitted with the model described above. We find variability of the overall flux, relatively minor changes in the degree of absorption, and distinct changes in the Fe ionization state. Fig. 6 shows 8 selected model spectra.

In the minimum (phase 0/1), there is a low ionization or neutral Fe absorption edge at $\sim 7 \text{ keV}$. On the other hand, a strongly ionized Fe absorption edge at $\sim 9 \text{ keV}$ is prominent in the maximum (phase 0.5). The edge energy and depth indicates the presence of a plasma with He-like Fe with the Thomson optical depth > 1 . Due to the low energy resolution of the PCA, it is impossible to determine the presence of any narrow absorption or emission spectral features.

A FIT TO BeppoSAX DATA

We then use a hard-state *BeppoSAX* observation from 1996 Sep. 22–24, closest in the spectral shape to our group 2 of Figs. 1–2. In this preliminary study, we fit only data from the MECS (which has energy resolution much better than that of the PCA), see Fig. 7. We find that the model described above gives a very poor fit with $\chi^2_{\nu} \sim 40$ as it cannot account for the discrete spectral features present in the $\sim 1.7\text{--}8 \text{ keV}$ band.

Thus, our new model consists of the Comptonization/reflection continuum (as above) and a component from a photoionized plasma, all absorbed in neutral

medium. The absorber includes both the interstellar medium and the wind from the companion, with the best-fit total $N_{\text{H}} \simeq 3.9 \times 10^{22} \text{ cm}^{-2}$. We also include an Fe $K\alpha$ line from an accretion disk [4]. The emission from the photoionized plasma (calculated using *xstar* [7]) turns out to be crucial. It improves the fit dramatically, to $\chi^2_{\nu} \simeq 1.6$. This is due to that component accounting for the strong emission features from highly ionized S, Si and Fe present in the MECS spectrum. Note that the *BeppoSAX* observation lasted more than nine orbital periods; thus, our results regard the phase-averaged spectrum.

This is our first, and preliminary, attempt of high resolution spectroscopy for Cyg X-3. We plan to apply our model to other *BeppoSAX* observations and those by *Chandra*.

CONCLUSIONS

We have obtained several major new results regarding X-rays from Cyg X-3, a preliminary account of them is given here. We have obtained the first classification of its X-ray spectra, forming 5 classes defined by the spectral hardness and the strength of the soft, disk-like component. Each class is well fitted by a physical model including Comptonization by both thermal and nonthermal electrons and Compton reflection. Apart from the presence of the very strong absorption in Cyg X-3, its intrinsic spectra are strikingly similar to those of the black-hole binary GRS 1915+105. This represents a strong argument for the presence of a black hole in Cyg X-3.

In the softest state, we have found a high-energy tail with $\Gamma \simeq 2$ extending above 100 keV . Such a spectral feature also appears in the brightest states of some other black-hole binaries, in particular GRS 1915+105 [17] and XTE J1550–564 [3]. The origin of this tail is probably due to Comptonization by nonthermal electrons.

We then present the *RXTE*/*ASM* lightcurve of this object, and obtain its profile folded over the orbital period. For the first time, we find distinct differences in its shape between the soft and hard states. This indicates some effects of the different X-ray emission on the surrounding absorbing medium causing the orbital modulation.

We also investigate the phase-resolved X-ray spectroscopy based on the PCA data. We find the $\sim 9 \text{ keV}$ edge from He-like Fe becomes strongest at the maximum, i.e., around the phase 0.5.

Last but not least, we fit the spectrum from an instrument with a medium energy resolution, the *BeppoSAX*/MECS. The spectrum, belonging to the hard state, shows a number of *emission* features, which we fit by a model of photoionized plasma. This component improves the fit to the data from $\chi^2_{\nu} \simeq 40$ to $\simeq 1.6$.

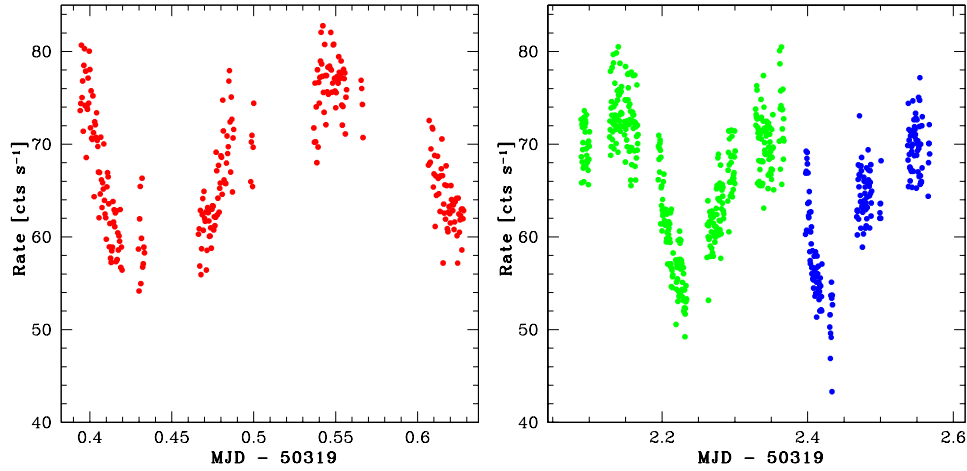


FIGURE 5. Example PCA lightcurves in the hard state, from observations on 1996 Aug. 24 and 26, left and right, respectively.

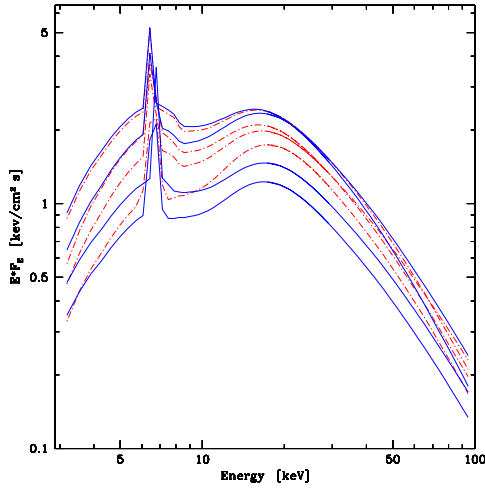


FIGURE 6. The Comptonization/reflection model fitted to the 8 (out of 18) phase-resolved spectra from Fig. 5. The dot-dashed (red) curves correspond to the phases of 0–0.5, and the solid (blue) curves, to the phases of 0.5–1.

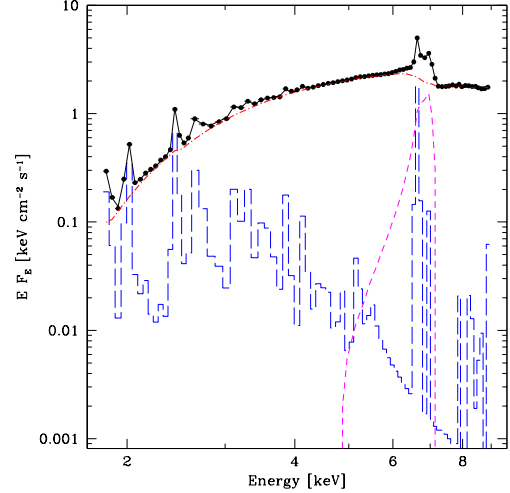


FIGURE 7. The *BeppoSAX*/MECS spectrum (dots/black) fitted by Comptonization/reflection (dot-dashes/red), Fe disk line (short dashes/magenta), emission of an ionized plasma (long dashes/blue), all absorbed by a neutral medium.

ACKNOWLEDGMENTS

This research has been supported in part by KBN grants 5P03D00821, 2P03C00619p1,2, and PBZ-KBN-054/P03/2001. We thank L. Hjalmarsdotter, P. Lachowicz, F. Paerels, and O. Vilhu for valuable discussions, and the *RXTE*/ASM team for their quick-look results.

REFERENCES

1. Belloni, T., et al., *A&A*, **355**, 271 (2000).
2. Coppi, P. S., ASP Conf. Ser. Vol. **161**, 375 (1999).

3. Done, C., *RSPTA*, **360**, 1967 (2002).
4. Fabian, A. C., et al., *MNRAS*, **238**, 729 (1989).
5. Giacconi, R., et al., *ApJ*, **148**, L119 (1967).
6. Gierliński, M., et al., *MNRAS*, **309**, 496 (1999).
7. Kallman, T. R., McCray, R., *ApJS*, **50**, 263 (1999).
8. Levine A. M., et al., *ApJ*, **469**, L33 (1996).
9. Magdziarz, P., Zdziarski, A. A., *MNRAS*, **273**, 837 (1995).
10. McCollough, M. L., et al, *NewAR*, **42**, 629 (1998).
11. McCollough, M. L., et al., *ApJ*, **517**, 951 (1999).
12. Poutanen, J., Svensson, R., *ApJ*, **470**, 249 (1996).
13. Predehl, P., et al., *A&A*, **357**, L25 (2000).
14. Singh, N. S., et al., *A&A*, **392**, 161 (2002).
15. van Keerkwijk, M. H., et al., *Nature*, **355**, 703 (1992).
16. Vilhu, O., et al., *A&A*, **411**, L405 (2003).
17. Zdziarski, A. A., et al., *ApJ*, **554**, L45 (2001).